Measurement of hadronic cross-sections with the *BABAR* detector

Marcus Ebert

on behalf of the *BABAR* Collaboration

University of Victoria, BC, Canada, V8N2X3

A program of measuring the light hadrons production in exclusive $e^+e^- \to$ hadrons processes is in place at *BABAR* with the aim to improve the calculation of the hadronic contribution to the muon $g-2$. We present the most recent results obtained by using the full data set of about $514 \, \mathrm{fb}^{-1}$ collected by the *BABAR* experiment at the PEP-II e^+e^- collider at a center-of-mass energy of about $10.6 \, \mathrm{GeV}$. In particular, we report the results on the channels $e^+e^- \to \pi^+\pi^-3\pi^0$, $e^+e^- \to \pi^+\pi^-2\pi^0\eta$, and its resonant sub-states. These final states are studied in a wide mass range, from threshold production up to about $4 \, \mathrm{GeV}/c^2$. In addition to the cross-sections, twelve J/ψ and $\psi(2S)$ branching fractions were measured with ten of them be a first-time measurement.

I. INTRODUCTION

Study of the $(g_\mu - 2)$ value show a discrepancy of about 3.7 standard deviation between the value measured in experiments and the value obtained from the Standard Model [1]. The calculation of the Standard Model value needs to account for hadronic vacuum polarization which is obtained from experimental e^+e^- hadronic cross-section measurements, especially within low-energy regions. So far not all accessible states have been measured and future measurements will improve the calculation of the Standard Model value for $(g_\mu - 2)$. Using initial-state radiation (ISR) processes give access to a wide range of different center-of-mass (CM) energies. In ISR events, the beam-energy in the CM system, $\sqrt{s}$, is reduced to a new CM energy, $\sqrt{s'}$, while the reduction depends on the value of the initial-state photon (fig.1). In addition, ISR events also allow resonance spectroscopy over a wide energy region.

BABAR is an e^+e^- collider experiment which has a rich ISR program and measured many different hadronic cross-sections in ISR events over the years. During the data taking period 1999-2008, *BABAR* collected $514 \, \mathrm{fb}^{-1}$ of data at CM energies equivalent to the mass of different $b\bar{b}$ resonances. *BABAR* published more than 580 papers over the years, and even thought it has been 11 years since *BABAR* stopped taking data there are still many ongoing analyses.

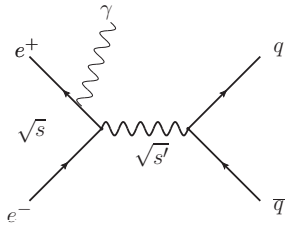In the analysis presented here, ISR events over an

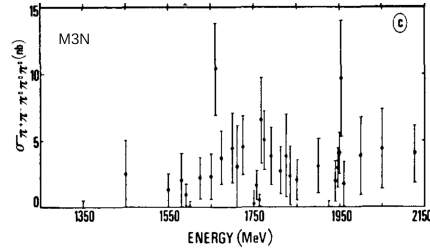FIG. 1: Emitting a photon in the initial state reduces $\sqrt{s}$ to $\sqrt{s'}$.

FIG. 2: Cross-section measurement of $e^+e^- \to \pi^+\pi^-3\pi^0$ by the M3N collaboration.

energy region from threshold up to the charmonium region are studied using the final states $\pi^+\pi^-2\pi^0\eta$ and $\pi^+\pi^-3\pi^0$, including its resonant sub-states.

II. ISR STUDY OF $e^+e^- \to \pi^+\pi^-3\pi^0$ AND $e^+e^- \to \pi^+\pi^-\pi^0\pi^0\eta$

A. Previous results

The cross-section for $e^+e^- \to \pi^+\pi^-3\pi^0$ was reported by M3N [2] and MEA [3] in 1979. While MEA reported only a single cross-section value over the whole energy range they studied, the M3N result is shown in fig.2. Recently, BESIII also showed a preliminary cross-section measurement for $e^+e^- \to \pi^+\pi^-3\pi^0$ [4], including the cross-section for the resonant sub-states (fig.3).

BABAR already measured the cross-section for $e^+e^- \to \eta\pi^+\pi^-$ with $\eta \to \pi^+\pi^-\pi^0$ and $\eta \to \gamma\gamma$. In this presentation, the cross-section measurement for the decay mode $e^+e^- \to \eta\pi^+\pi^-$ with $\eta \to 3\pi^0$ as a resonant sub-state of $e^+e^- \to \pi^+\pi^-3\pi^0$ is presented.

A measurement for the cross section of $e^+e^- \to \pi^+\pi^-\pi^0\pi^0\eta$ has not been reported by another experiment so far. The SND Collaboration however reported cross-section measurements for the resonant sub-modes $e^+e^- \to \omega\pi^0\eta$ and $e^+e^- \to \phi\pi^0\eta$.
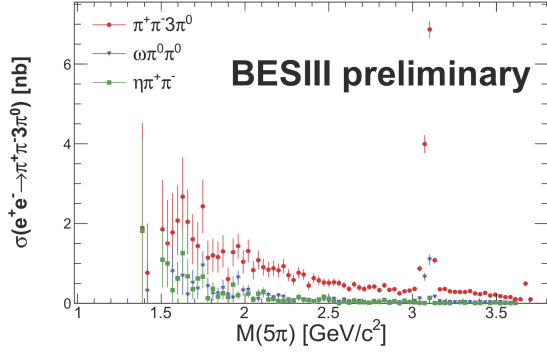
FIG. 3: Preliminary cross-section measurement of $e^+e^- \to \pi^+\pi^-3\pi^0$ by the BESIII collaboration.

FIG. 4: Invariant $\gamma\gamma$ mass distribution in $e^+e^- \to \pi\pi^-\pi^0\pi^0\gamma\gamma$ ISR events obtain in the signal region(blue) and the control region (red), as well as background events from $e^+e^- \to \pi^+\pi^-\pi^0\pi^0$ (green).

B. Selection criteria

For the selection of events of interest, two well reconstructed tracks are required. Those tracks are fitted to a common vertex which needs to be close to the collision point of the beams. In addition, both tracks need to be inconsistent with being a kaon or muon. Also, each event needs to have at least seven photons. At least one photon needs to have an energy of more than 3 GeV and it is assumed that the photon with the highest energy is the ISR photon. The additional six photons are combined into three pairs resulting in fifteen combinations when all possible combinations are considered. At least two of those pairs, the π^0 candidates, need to have a mass that is within $35 \, \text{MeV}/c^2$ around the π^0-mass, $\|m_{\pi^0_{\text{cand}}} - m_{\pi^0}\| < 35 \, \text{MeV}/c^2$. There is no constraint placed on the third pair which allows to reconstruct the final state with $3\pi^0$ as well as the final state with $2\pi^0\eta$. A kinematic fit is performed on the the whole event, $e^+e^- \to \pi^+\pi^-2\pi^0\gamma\gamma\gamma_{\text{ISR}}$, with the following conditions:

- the mass of the π^0 candidates, $m_{\pi^0_{\text{cand}}}$, is constrained to the mass of a π^0, m_{π^0},

- $\chi^2_{\pi^+\pi^-\pi^0\pi^0\gamma\gamma}$, obtained from the kinematic fit, needs to be smaller than 60, and

- the combination of candidates that gives the smallest χ^2 in this fit will be used.

In addition, a control region is defined as the region where $\chi^2_{\pi^+\pi^-\pi^0\pi^0\gamma\gamma}$ is greater than 60 and smaller than 120.

C. Background reduction

The main background comes from $\tau^+\tau^-$ decays, from $e^+e^- \to \pi^+\pi^-\pi^0\pi^0\gamma_{\text{ISR}}$ events, and from non-ISR uds events. To suppress background from $\tau^+\tau^-$ decays, charged tracks are required to be not too close to the ISR photon.
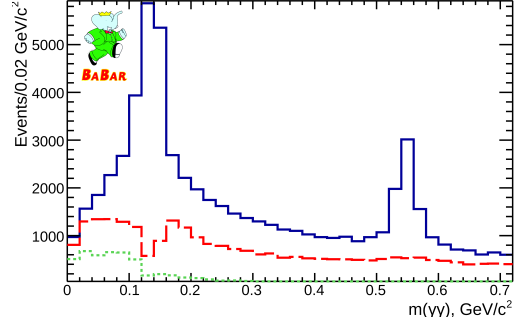
The cross-section for the ISR mode $e^+e^- \to \pi^+\pi^-\pi^0\pi^0$ is expected to be larger than for the studied decay modes. When there are two additional background photons in the event, then it could appear to be a signal in one of the studied decay modes. To suppress those events, a kinematic fit is also performed for this final state and events with $\chi^2_{\pi^+\pi^-\pi^0\pi^0\gamma_{\text{ISR}}} < 30$ are rejected.

The non-ISR event $e^+e^- \to \pi^+\pi^-\pi^0\pi^0\pi^0\pi^0$ could also appear as a signal when one of the π^0 decays in a way that one of the two photons is very high energetic. In this case, this high-energy photon would be misidentified as the ISR-photon. Since the second photon has a very low energy in this case, those events would look like signal. Therefore this kind of background is taken into account when determining in the cross-section.

D. Signal extraction

By varying the required ISR-photon energy in 50 MeV steps, $\sqrt{s'}$ is scanned from threshold up to the charmonium region. In each 50 MeV interval, the signal is then extracted as described in this subsection.

The signal extraction for the modes $e^+e^- \to \pi^+\pi^-3\pi^0$ and $e^+e^- \to \pi^+\pi^-2\pi^0\eta$ is done in the invariant mass distribution of the third $\gamma\gamma$ pair. In each interval, the $m(\gamma\gamma)$ distribution from the χ^2 control region is subtracted from the signal distribution and the resulting distribution fitted for the number of π^0 or η, depending on the final state. In those fits, the signal shape is fixed to the one obtained from simulated signal events. Figure 4 shows the $m(\gamma\gamma)$ distribution for all energy intervals combined and fig.5 the fit to obtain the number of π^0 after subtracting the control region distribution.

When studying resonant sub-modes, the same procedure is used but the number of signal events in each interval is obtained from a fit to the invariant mass
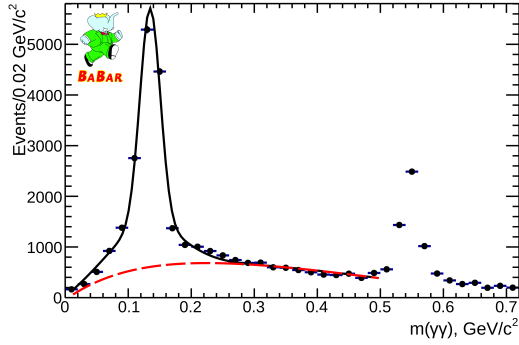
FIG. 5: $m(\gamma\gamma)$ distribution after subtracting the distribution from the control region (black markers) fitted for the number of π^0 (black line) and background (red).
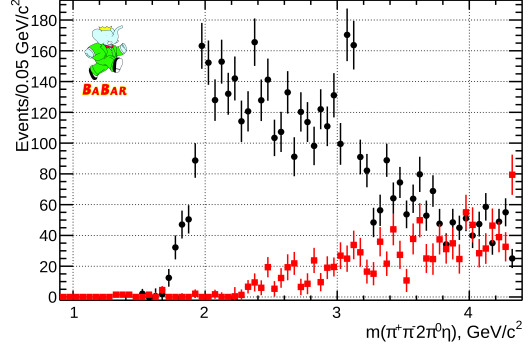

FIG. 7: Invariant mass distribution of $e^+e^- \to \pi^+\pi^- 2\pi^0\eta$ ISR events (black) and background from non-ISR events (red).
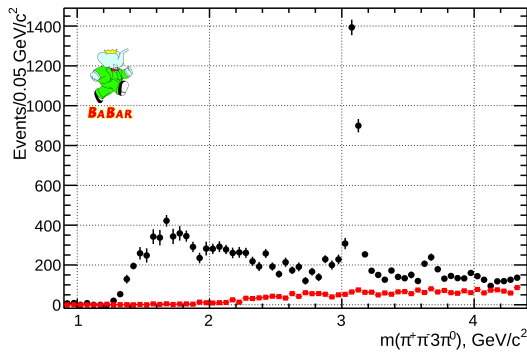

FIG. 6: Invariant mass distribution of $e^+e^- \to \pi^+\pi^- 3\pi^0$ ISR events (black) and background from non-ISR events (red).
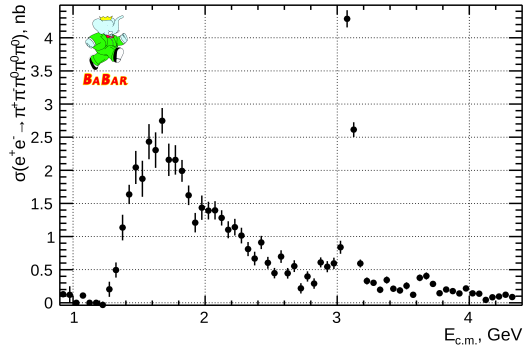

FIG. 8: Cross-section for $e^+e^- \to \pi^+\pi^- 3\pi^0$ ISR events in 50 MeV intervals in $\sqrt{s'}$ ($E_{\mathrm{c.m.'}}$).

distribution that shows the resonance. The obtained signal yields are then used to determine the cross-sections.

III. RESULTS

A. $\pi^+\pi^- 3\pi^0$ and $\pi^+\pi^- 2\pi^0\eta$ final states

Using the fit results for the number of signal events from each $\sqrt{s'}$ interval, a signal distribution over the whole accessible energy range is obtained for each final state. Those distributions are shown for the $\pi^+\pi^- 3\pi^0$ final state in fig.6 and for the $\pi^+\pi^- 2\pi^0\eta$ final state in fig.7. Those distributions are then used to determine the cross-section for each interval, also taking the additional background contributions into account. The resulting cross-section distributions are shown in fig.8 and in fig.9.

B. $\pi^+\pi^-\eta$ and $\omega\pi^0\pi^0$ final states

The $\pi^+\pi^-\eta$ and $\omega\pi^0\pi^0$ final states are resonant substates for the already shown final state $\pi^+\pi^- 3\pi^0$ and therefore included in the result of the previous subsection. The number of events in each energy interval
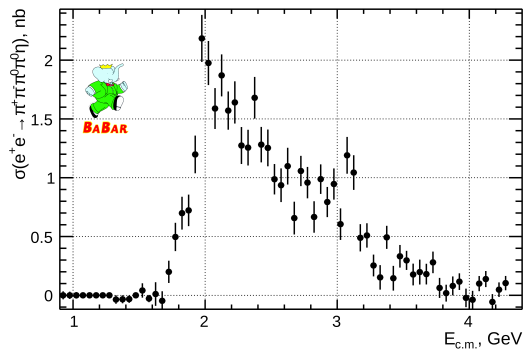

FIG. 9: Cross-section for $e^+e^- \to \pi^+\pi^- 2\pi^0\eta$ ISR events in 50 MeV intervals in $\sqrt{s'}$ ($E_{\mathrm{c.m.'}}$).
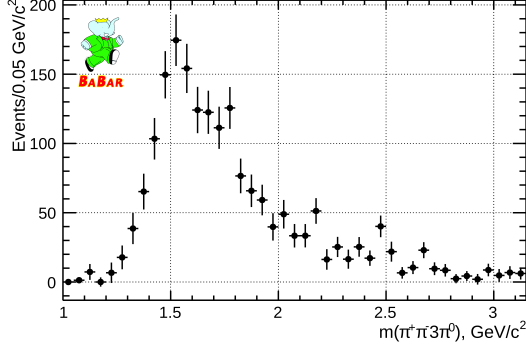
FIG. 10: Invariant mass distribution $m(\pi^+\pi^-3\pi^0)$ for $e^+e^- \to \pi^+\pi^-\eta, \eta \to 3\pi^0$ ISR events.

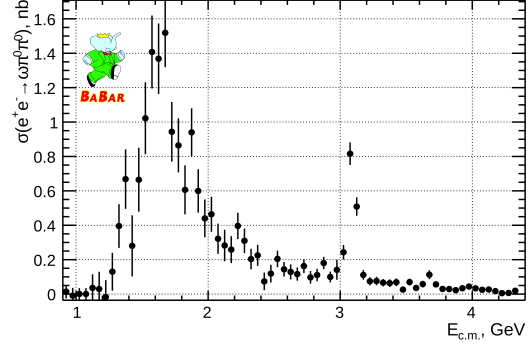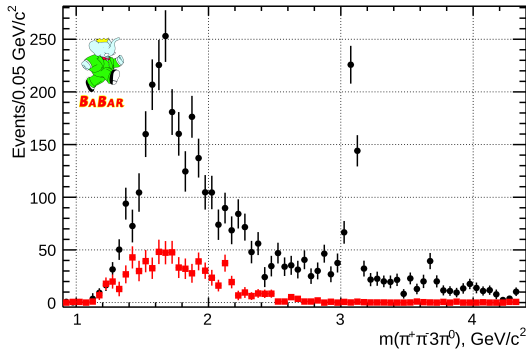FIG. 11: Invariant mass distribution $m(\pi^+\pi^-3\pi^0)$ for $e^+e^- \to \omega\pi^0\pi^0, \omega \to \pi^+\pi^-\pi^0$ ISR events (black) and background from $e^+e^- \to \omega\pi^0$ events.

for both final states is shown in fig.10 and fig.11. The resulting cross-section distributions over the whole accessible energy range in fig.12 and fig.13.

In addition to those two sub-modes, also finale states with ρ contribute to $e^+e^- \to \pi^+\pi^-3\pi^0$. Contributions from the final states $\rho^\pm\pi^\mp2\pi^0$ and $\rho^+\rho^-\pi^0$

FIG. 12: Cross-section for $e^+e^- \to \pi^+\pi^-\eta$ ISR events in 50 MeV intervals in $\sqrt{s'}$ ($E_{\text{c.m.'}}$).

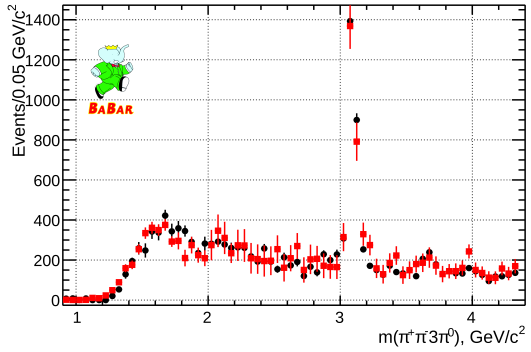FIG. 13: Cross-section for $e^+e^- \to \omega\pi^0\pi^0$ ISR events in 50 MeV intervals in $\sqrt{s'}$ ($E_{\text{c.m.'}}$).

FIG. 14: Invariant mass distribution $m(\pi^+\pi^-3\pi^0)$ for $e^+e^- \to \pi^+\pi^-3\pi^0$ ISR events (black) and for the sum of all resonant sub-modes (red).

have been found but are not shown in this conference proceeding for space reasons.

Interesting to note is that the sum of all resonant contributions account for the total number of events found for the final state $\pi^+\pi^-3\pi^0$. This is shown in fig.14. Therefore it appears that only resonant sub-modes contribute to the $e^+e^- \to \pi^+\pi^-3\pi^0$ in the studied energy region.

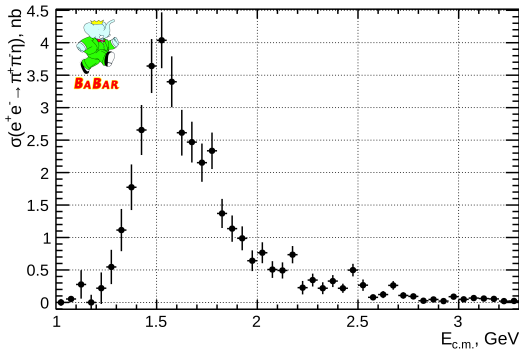### C. $\omega\pi^0\eta$ and $\phi\pi^0\eta$ final states

The $\omega\pi^0\eta$ and $\phi\pi^0\eta$ final states are resonant sub-states for the previously shown final state $\pi^+\pi^-2\pi^0\eta$ and include in those measurements. Figure 15 shows the $m(\pi^+\pi^-\pi^0)$ distribution from which the signal yields for both resonances are extracted by a combined fit. The cross-section result is shown in fig.16 together with the results obtained by the SND collaboration.
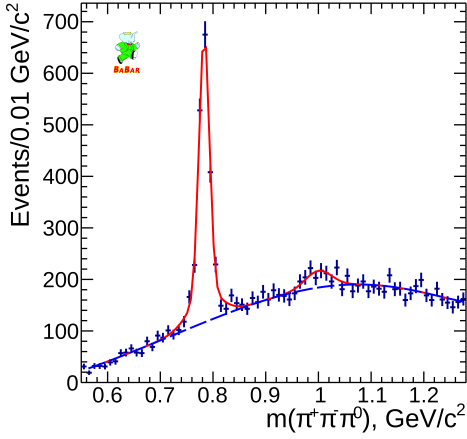
FIG. 15: Fit to the invariant mass distribution $m(\pi^+\pi^-\pi^0)$ (black) to extract the ω and ϕ yields (red).
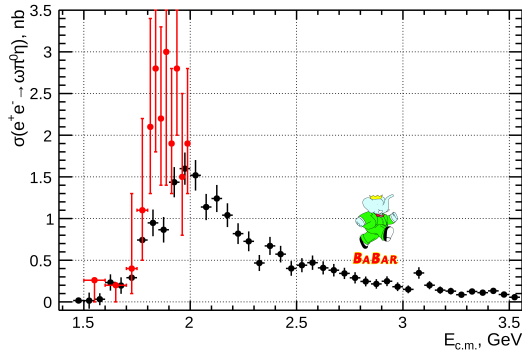

FIG. 16: Cross-section measurement for $e^+e^- \to \omega\pi^0\eta$ by *BABAR* (black) and the SND Collaboration (red).

D. J/ψ and $\psi(2S)$ branching fractions

When looking to the previously shown distribution of signal events in the different final states, the J/ψ and $\psi(2S)$ resonances are also seen. As an example, fig. 17 to 19 show the signal event distribution for different modes around the J/ψ and $\psi(2S)$ mass. By fitting those distributions for the number of J/ψ or $\psi(2S)$ candidates, one can determine the branching fraction for different decay modes of those resonances. This was done for 12 different modes, shown in table I, while only two of them were known before.

IV. CONCLUSION

Although the *BABAR* collaboration stopped data taking 11 years ago, it still has a rich ongoing physics program and publishes results of which some are even first time measurements. In this presentation, hadronic cross-section distributions were presented for
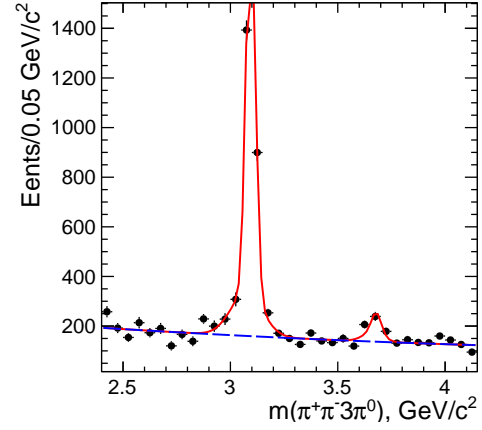
FIG. 17: Invariant mass distribution $m(\pi^+\pi^-3\pi^0)$ (black), fitted to extract the number of J/ψ and $\psi(2S)$ candidates (red).
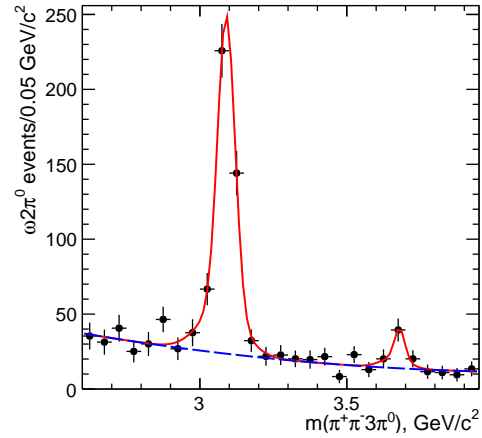

FIG. 18: Invariant mass distribution $m(\omega 2\pi^0, \omega \to \pi^+\pi^-\pi^0)$ (black), fitted to extract the number of J/ψ and $\psi(2S)$ candidates (red).
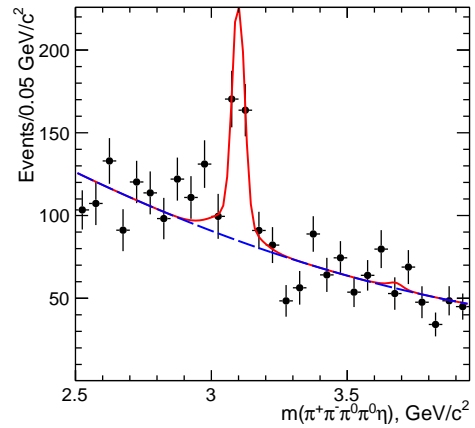

FIG. 19: Invariant mass distribution $m(\pi^+\pi^-2\pi^0\eta)$ (black), fitted to extract the number of J/ψ and $\psi(2S)$ candidates (red).

Measured Quantity	Measured Value (eV)	J/ψ or $\psi(2S)$ Branching Fraction (10^{-3})	
		this analysis [5]	previously known [1]
$\Gamma_{ee}^{J/\psi} \cdot \mathcal{B}_{J/\psi \to \pi^+\pi^-\pi^0\pi^0\pi^0}$	$150.0\pm4.0\pm15.0$	$27.0\ \pm0.7\ \pm2.7$	no entry
$\Gamma_{ee}^{J/\psi} \cdot \mathcal{B}_{J/\psi \to \omega\pi^0\pi^0} \cdot \mathcal{B}_{\omega \to 3\pi}$	$24.8\pm1.8\pm2.5$	$5.04\pm0.37\pm0.50$	3.4 ± 0.8
$\Gamma_{ee}^{J/\psi} \cdot \mathcal{B}_{J/\psi \to \rho^\pm\pi^\mp\pi^0\pi^0}$	$78.0\pm9.0\pm8.0$	$14.0\ \pm1.2\ \pm1.4$	no entry
$\Gamma_{ee}^{J/\psi} \cdot \mathcal{B}_{J/\psi \to \rho^+\rho^-\pi^0}$	$33.0\pm5.0\pm3.3$	$6.0\ \pm0.9\ \pm0.6$	no entry
$\Gamma_{ee}^{J/\psi} \cdot \mathcal{B}_{J/\psi \to \pi^+\pi^-\pi^0\pi^0\eta}$	$12.8\pm1.8\pm2.0$	$2.30\pm0.33\pm0.35$	no entry
$\Gamma_{ee}^{J/\psi} \cdot \mathcal{B}_{J/\psi \to \omega\pi^0\eta} \cdot \mathcal{B}_{\omega \to 3\pi}$	$1.7\pm0.8\pm0.3$	$0.34\pm0.16\pm0.06$	no entry
$\Gamma_{ee}^{J/\psi} \cdot \mathcal{B}_{J/\psi \to \rho^\pm\pi^\mp\pi^0\eta}$	$10.5\pm4.1\pm1.6$	$1.7\ \pm0.7\ \pm0.3$	no entry
$\Gamma_{ee}^{\psi(2S)} \cdot \mathcal{B}_{\psi(2S) \to \pi^+\pi^-\pi^0\pi^0\pi^0}$	$12.4\pm1.8\pm1.2$	$5.2\ \pm0.8\ \pm0.5$	no entry
$\Gamma_{ee}^{\psi(2S)} \cdot \mathcal{B}_{\psi(2S) \to J/\psi\pi^0\pi^0} \cdot \mathcal{B}_{J/\psi \to 3\pi}$	$10.1\pm1.5\pm1.1$	$22.9\ \pm2.8\ \pm2.3$	21.1 ± 0.7
$\Gamma_{ee}^{\psi(2S)} \cdot \mathcal{B}_{\psi(2S) \to \omega\pi^0\pi^0} \cdot \mathcal{B}_{\omega \to 3\pi}$	$2.3\pm0.7\pm0.2$	$1.1\ \pm0.3\ \pm0.1$	no entry
$\Gamma_{ee}^{\psi(2S)} \cdot \mathcal{B}_{\psi(2S) \to \rho^\pm\pi^\mp\pi^0\pi^0}$	<6.2 at 90% C.L.	<2.6 at 90% C.L.	no entry
$\Gamma_{ee}^{\psi(2S)} \cdot \mathcal{B}_{\psi(2S) \to \pi^+\pi^-\pi^0\pi^0\eta}$	<0.85 at 90% C.L.	<0.35 at 90% C.L.	no entry

TABLE I: Summary of the measured J/ψ and $\psi(2S)$ branching fractions.

different final states obtained from ISR events over a large energy region. These new measurements show an increased precision over previous measurements, where previous measurement exist. The presented measurement for the cross-section of the final state $\pi^+\pi^-2\pi^0\eta$ was a first time measurement for this final state.

In addition, twelve branching fraction measurements for different decay modes of the J/ψ and $\psi(2S)$ resonances were presented. Only two of them were previously known.

The analyses that measured those cross-sections and branching fractions is published in Phys. Rev. D. More details about it as well as tables with all measured cross-sections can be found in [5].

---

[1] M. Tanabashi *et al.* (Particle Data Group), Phys. Rev. D**98**, 030001 (2018).
[2] G. Cosme *et al.*, Nucl. Phys. B **152**, 215 (1979).
[3] B. Esposito *et al.*, Lett. Nuovo Cim. **25**, 5 (1979).
[4] M. Ripka *et al.*, Nucl.Part.Phys.Proc. **294-296**, 158-163 (2018).
[5] J.P.Lees *et al.*, Phys. Rev. D **98**, 112015 (2018).